








RESEARCH ARTICLE | SEPTEMBER 12 2023

The ^{103}Rh NMR spectroscopy and relaxometry of the rhodium formate paddlewheel complex

Harry Harbor-Collins ; Mohamed Sabba ; Gamal Moustafa; Bonifac Legrady ; Murari Soundararajan ; Markus Leutzsch ; Malcolm H. Levitt  



J. Chem. Phys. 159, 104307 (2023)

<https://doi.org/10.1063/5.0165830>



View
Online



Export
Citation

CrossMark

The ^{103}Rh NMR spectroscopy and relaxometry of the rhodium formate paddlewheel complex

Cite as: J. Chem. Phys. 159, 104307 (2023); doi: 10.1063/5.0165830

Submitted: 30 June 2023 • Accepted: 15 August 2023 •

Published Online: 12 September 2023



View Online



Export Citation



CrossMark

Harry Harbor-Collins,¹ Mohamed Sabba,¹ Gamal Moustafa,¹ Bonifac Legrady,¹ Murari Soundararajan,¹ Markus Leutzsch,² and Malcolm H. Levitt^{1,a)}

AFFILIATIONS

¹School of Chemistry, University of Southampton, Southampton SO17 1BJ, United Kingdom

²Max-Planck-Institut für Kohlenforschung, Kaiser-Wilhelm-Platz 1, Mülheim an der Ruhr 45470, Germany

^{a)}Author to whom correspondence should be addressed: mhl@soton.ac.uk

ABSTRACT

The nuclear magnetic resonance (NMR) spectroscopy of spin-1/2 nuclei with low gyromagnetic ratio is challenging due to the low NMR signal strength. Methodology for the rapid acquisition of ^{103}Rh NMR parameters is demonstrated for the case of the rhodium formate “paddlewheel” complex $\text{Rh}_2(\text{HCO}_2)_4$. A scheme is described for enhancing the ^{103}Rh signal strength by polarization transfer from ^1H nuclei, which also greatly reduces the interference from ringing artifacts, a common hurdle for the direct observation of low- γ nuclei. The ^{103}Rh relaxation time constants T_1 and T_2 are measured within 20 min by using ^1H -detected experiments. The field dependence of the ^{103}Rh T_1 is measured. The high-field relaxation is dominated by the chemical shift anisotropy mechanism. The ^{103}Rh shielding anisotropy is found to be very large: $|\Delta\sigma| = 9900 \pm 540$ ppm. This estimate is compared with density functional theory calculations.

© 2023 Author(s). All article content, except where otherwise noted, is licensed under a Creative Commons Attribution (CC BY) license (<http://creativecommons.org/licenses/by/4.0/>). <https://doi.org/10.1063/5.0165830>

I. INTRODUCTION

Rhodium paddlewheel complexes have attracted significant attention due to their unique properties and diverse applications where they have played roles as catalysts and potential anticancer agents.^{1–5} These complexes consist of two rhodium atoms bridged by four carboxylate ligands, forming a lantern-like structure, with some resemblance to the paddlewheels of a river boat. A typical example is rhodium formate, $\text{Rh}_2(\text{HCO}_2)_4$, see Fig. 1.

Nuclear magnetic resonance (NMR) is a powerful probe of the properties of rhodium complexes. ^{103}Rh carries the distinction of being one of only 4 (with ^{19}F , ^{31}P , and ^{89}Y) spin-1/2 nuclei with a natural abundance of 100%. Nevertheless, it has been relatively neglected by spectroscopists: ^{103}Rh is a member of what Mann dubbed “the Cinderella nuclei”⁶—transition metals with spin-1/2 but very low magnetogyric ratio γ . The NMR of ^{103}Rh is associated with multiple experimental challenges leading to a relative scarcity of experimental data. However, many of these challenges have been successfully overcome by the creative application of modern NMR methodology, such as heteronuclear multiple-quantum (HMQC) NMR.⁷ However, although HMQC experiments allow the rapid acquisition of ^{103}Rh NMR spectra in suitable cases, it is not possible

to estimate ^{103}Rh spin-lattice and spin-spin relaxation time constants through HMQC experiments. For this purpose, experiments exploiting ^{103}Rh magnetization are needed.

In this work, we utilize a variant of the PulsePol polarization transfer technique^{8–10} to enhance the ^{103}Rh NMR spectroscopy of the rhodium formate paddlewheel complex in solution. We report the following: (i) NMR methodology for the acquisition of directly detected ^{103}Rh spectra with effective ringing filtration and (ii) NMR methodology for the rapid measurement of ^{103}Rh T_1 and T_2 relaxation time constants over a range of magnetic field strengths. We observe a strong field dependence of the ^{103}Rh T_1 , which is qualitatively consistent with a dominant chemical shift anisotropy (CSA) relaxation mechanism. We estimate the ^{103}Rh shielding anisotropy by using information from ^{13}C and ^{103}Rh relaxation experiments in solution and from ^{13}C solid-state NMR.

II. EXPERIMENTAL

A. Sample

Experiments were performed on a saturated (~10 mM) solution of rhodium formate ($\text{Rh}_2(\text{HCO}_2)_4$) dissolved in 500 μl deuterated

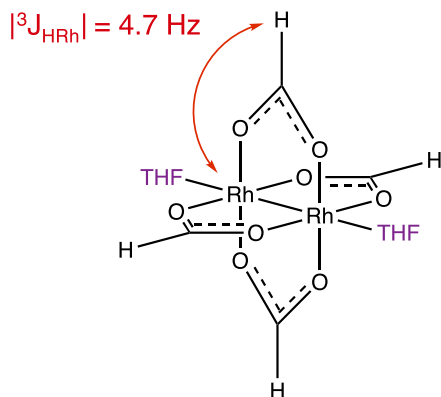


FIG. 1. Molecular structure of the rhodium formate paddlewheel complex ligated by solvent tetrahydrofuran (THF) molecules at the axial sites. This work exploits the ${}^3J_{\text{RhH}}$ scalar couplings for polarization transfer between the ${}^{103}\text{Rh}$ and ${}^1\text{H}$ nuclei.

tetrahydrofuran (THF- d_8) contained in a Wilmad LPV 5 ml sample tube. The rhodium formate was synthesized from rhodium chloride using a reported procedure¹¹ and dried extensively under heated vacuum. The resulting rhodium formate solid was green in color and dissolved in THF to produce a green solution.

B. Solution NMR

${}^1\text{H}$ and ${}^{103}\text{Rh}$ spectra were acquired at a magnetic field strength of 9.4 T using a standard commercial Bruker 5 mm NMR BBO probe (${}^1\text{H}/{}^2\text{H}/{}^{109}\text{Ag}-{}^{31}\text{P}$) equipped with a z-gradient with a maximum strength of 50 G cm^{-1} .

Proton resonances are referenced to the absolute frequency $400.143\,00\text{ MHz}$, whereas ${}^{103}\text{Rh}$ resonances are referenced to an absolute frequency that is proportional to the protons [$\Xi({}^{103}\text{Rh}) = 3.16\%$] per the most common convention.¹²

Although the probe could be tuned to ${}^{103}\text{Rh}$ beyond the manufacturer specifications, it was set to mismatched (overcoupled) conditions to reduce ringdown times.^{13–16} The radio frequency amplitudes on the ${}^1\text{H}$ and ${}^{103}\text{Rh}$ channels were both adjusted to give an intentionally matched nutation frequency of $\omega_{\text{nut}}/(2\pi) \approx 4\text{ kHz}$, corresponding to a 90° pulse duration of $62.5\ \mu\text{s}$.

Additional isolation of the rf channels by electronic filters was found to be necessary—without the filters, noise on the ${}^{103}\text{Rh}$ channel was significant enough to preclude observation of other nuclei. At the preamplifier output, we installed: a 30 MHz lowpass filter (Chemagnetics) on the ${}^{103}\text{Rh}$ channel, a 400 MHz bandpass filter (K & L Microwave) on the ${}^1\text{H}$ channel, and a 61 MHz bandpass filter (FSY Microwave) on the ${}^2\text{H}$ lock channel.

To measure relaxation times as a function of the magnetic field, the experiments used rapid sample shuttling from inside the 9.4 T magnet bore to regions of lower field outside the magnet bore.¹⁷ The shuttling was performed using a motorized fast shuttling system based on the design by Kiryutin.¹⁸ The shuttling time was kept constant at 1 s.

The pulse sequences described below use the following elements:

1. Composite pulses

Composite pulses were used to minimize the effects of rf field inhomogeneity and are denoted by shaded black rectangles in the pulse sequence diagrams. All composite pulses are implemented using the symmetrized BB1 composite pulse scheme^{19,20} in which a simple pulse β_ϕ (where β is the flip angle and ϕ is the phase) is replaced by

$$(\beta/2)_\phi 180_{\phi+\theta_W} 360_{\phi+3\theta_W} 180_{\phi+\theta_W} (\beta/2)_\phi, \quad (1)$$

where $\theta_W = \arccos(-\beta/(4\pi))$. For the $\pi/2$ and π flip angles used in this paper, this corresponds to the following sequences:

$$90_\phi \rightarrow 45_\phi 180_{\phi+97.18} 360_{\phi+291.54} 180_{\phi+97.18} 45_\phi, \quad (2)$$

$$180_\phi \rightarrow 90_\phi 180_{\phi+104.48} 360_{\phi+313.43} 180_{\phi+104.48} 90_\phi. \quad (3)$$

2. DualPol polarization transfer sequence

The transfer of polarization between ${}^{103}\text{Rh}$ and ${}^1\text{H}$ was achieved using the pulse sequence shown in Fig. 2. This consists of repeating PulsePol sequences,^{8,9} applied simultaneously to the ${}^1\text{H}$ and ${}^{103}\text{Rh}$ radio frequency channels. The PulsePol sequence consists of six phase-shifted radio frequency pulses and four intervals τ , and was originally developed for polarization transfer between electron and nuclear spins in the context of nitrogen-vacancy diamond magnetometry.⁸ It has also been shown to be effective for singlet-to-magnetization conversion^{9,10} and has been interpreted in terms of symmetry-based recoupling theory.¹⁰ For convenience, we refer to the “dual PulsePol” sequence in Fig. 2 as “DualPol.”

DualPol is an unusual example of a solution-state polarization transfer sequence combining (i) multiple-pulse averaging^{22,23} and (ii) hard pulses separated by delays. The sequence provides robust polarization transfer even in the strong-coupling regime, where the standard INEPT sequence breaks down.^{24–28} That particular feature is not essential for the results described here. However, it is

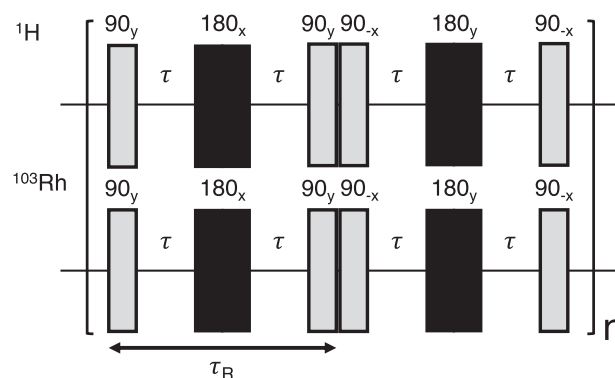


FIG. 2. DualPol pulse sequence used for ${}^1\text{H}$ – ${}^{103}\text{Rh}$ cross polarization, consisting of simultaneous PulsePol sequences⁸ on the two channels. Each PulsePol sequence is a repeating sequence of two R-elements. Each R-element has duration τ_R and is given by a composite 180° pulse²¹ with delays of duration τ between the pulses. The R-element duration should be short compared to the inverse of the relevant J-couplings. The black rectangles indicate BB1 composite π -pulses [Eq. (3)].

advantageous in other circumstances, as will be discussed in a future publication.

The repeating sequences of PulsePol and DualPol are composed of three-pulse elements of the form $90_y 180_x 90_x$, with the pulses separated by intervals τ , and variants thereof. Each three-pulse sequence is, therefore, a “windowed” version of a composite 180° pulse.²¹ Therefore, we call this three-pulse sequence a “R-element,” using notation originally introduced in the context of broadband heteronuclear decoupling,²⁹ and later adapted for symmetry-based recoupling sequences in solid-state NMR³⁰ and symmetry-based singlet-triplet conversion sequences in solution NMR.¹⁰ In the case of DualPol, there is no special constraint or matching condition on the duration τ_R of the R-element, except that it should be much shorter than the period of the relevant J-coupling, $\tau_R \ll |^3J_{\text{RhH}}|^{-1}$. Under these conditions, the average Hamiltonian²² generated by the DualPol sequence, for a heteronuclear two-spin system, has the form

$$\bar{H}^{(1)} \simeq \kappa_{\text{DP}} \times 2\pi J_{\text{IS}} (I_x S_x + I_y S_y), \quad (4)$$

where the nuclides ^1H and ^{103}Rh are referred to as I and S , respectively. The numbering convention for the average Hamiltonian terms starts with 1 for the lowest order approximation, in common with the symmetry-based recoupling literature.³⁰ The DualPol scaling factor is given, under suitable approximations, by $\kappa_{\text{DP}} \simeq \frac{1}{2}$ in the limit of strong radio frequency pulses. Equation (4) corresponds to an anisotropic Hartmann–Hahn Hamiltonian,³¹ indicating that the DualPol sequence exchanges z -magnetization components between the I -spins and S -spins. The theory and performance of the DualPol sequence will be discussed in more depth in a future paper.

In the experiments described here, all DualPol sequences used an R-element duration of $\tau_R = 5$ ms and a repetition number of $n = 10$. The total duration of each DualPol sequence was $T = 2n\tau_R = 100$ ms.

3. ^1H destruction filter

The ^1H destruction filter is shown in Fig. 3. The filter has the net effect of dephasing residual proton transverse and longitudinal magnetizations (which may be generated by accidental excitation and recovery during the decay interval, respectively).

4. ^1H z-filter

The z-filter for the selection of longitudinal ^1H magnetization is shown in Fig. 4. This employs a bipolar gradient scheme in order to reduce spectral distortions by eddy currents or residual gradient fields.³²

C. Solid-state NMR

Solid-state CPMAS ^{13}C NMR was performed using a 4 mm Bruker probe at 14.1 T and ~ 303 K.

D. Computational chemistry

Quantum chemical geometry optimization and shielding tensor calculations for the rhodium formate complex axially ligated by solvent THF molecules were performed using the ORCA program package version 5.0.3.³³ ^{103}Rh shielding tensors were computed at the TPSSh/SARC-ZORA-TZVPP level of theory.

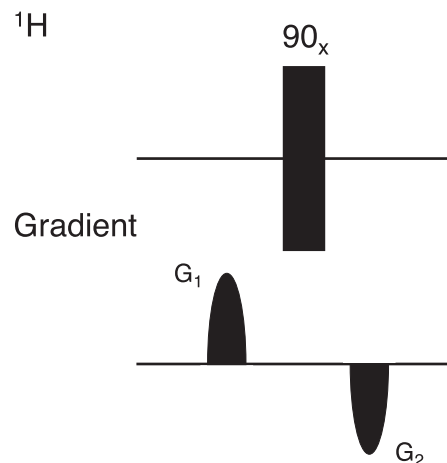


FIG. 3. Proton destruction filter for the removal of residual proton magnetization. The gradient strengths are given by $G_1 = 100\%$ and $G_2 = -61.8\%$ with respect to the maximum gradient strength 50 G cm^{-1} . Each gradient has a duration of 2 ms. The black rectangle indicates a BB1 composite $\pi/2$ pulse [Eq. (2)].

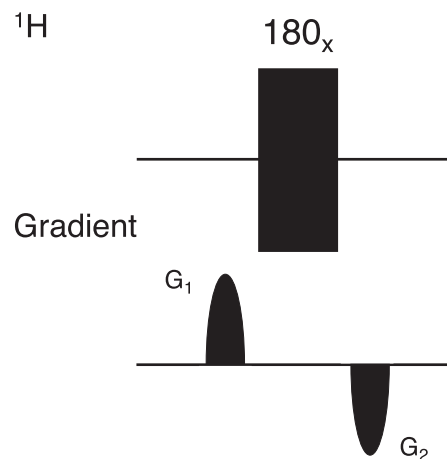


FIG. 4. Proton z-filter for the selection of proton z -magnetization using bipolar gradients. The gradient strengths are given by $G_1 = 40\%$ and $G_2 = -40\%$ with respect to the maximum gradient strength of 50 G cm^{-1} . Each gradient pulse has a duration of 2 ms. The black rectangle indicates a BB1 composite π -pulse [Eq. (3)].

III. RESULTS

A. NMR spectra

1. Solution-state ^1H spectrum

The rhodium formate ^1H spectrum features a single formate ^1H resonance split into a 1:2:1 triplet by coupling to the pair of magnetically equivalent ^{103}Rh nuclei (Fig. 5). The three-bond ^1H - ^{103}Rh J-coupling is estimated to be $|^3J_{\text{RhH}}| = 4.7 \pm 0.1 \text{ Hz}$.

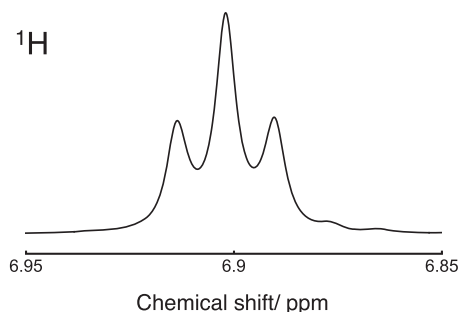


FIG. 5. ^1H spectrum of a ~ 10 mM solution of rhodium formate in THF-d_8 , acquired at 9.4 T and at 298 K in a single scan. Exponential line broadening (0.75 Hz) was applied.

2. Solution-state ^{103}Rh spectra

The sequence shown in Fig. 6 was used for the acquisition of directly detected ^{103}Rh spectra, enhanced by polarization transfer from ^1H nuclei. After an initial pair of 90° pulses, used for the suppression of ringing artifacts (see below), the DualPol sequence transfers z-magnetization from the ^1H to the ^{103}Rh nuclei, exploiting the form of the DualPol average Hamiltonian [Eq. (4)]. The resultant ^{103}Rh z-magnetization is converted into observable transverse magnetization by a final 90° pulse. The ^{103}Rh NMR signal is enhanced by a factor of up to $|\gamma_I/\gamma_S| \sim 31$, relative to that induced by a single 90° pulse applied to ^{103}Rh nuclei in thermal equilibrium.

Ringing artifacts are strongly suppressed by a phase-cycled pair of 90° pulses on the proton channel, before the polarization transfer takes place. The signs of the ^1H magnetization and the ^{103}Rh receiver are simultaneously inverted in successive scans. Since the phases of the ringing are correlated with the phases of the pulses on the ^{103}Rh channel, the ringing is strongly suppressed in the ^{103}Rh spectrum. Further suppression of ringing is achieved by additional phase cycling of the PulsePol blocks. The sign of the ^{103}Rh magnetization is invariant under global phase shifts of the DualPol sequence, while the ringing contribution is phase-correlated and largely cancels out. Similar logic has been used to design excitation schemes for ringing suppression in homonuclear NMR experiments.^{34,35}

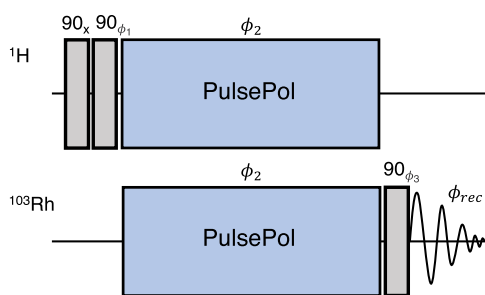


FIG. 6. Pulse sequence for the acquisition of ^1H enhanced ^{103}Rh spectra. A 16-step phase cycle is used where $\phi_1 = [-x, x, -x, x]$, $\phi_2 = [x, x, -x, -x]$, $\phi_3 = [x, x, x, x, y, y, y, y, -x, -x, -x, -x, -y, -y, -y, -y]$ and the receiver $\phi_{rec} = [x, -x, x, -x, y, -y, y, -y, -x, x, -x, x, -y, y, -y, y]$, all of which combine to suppress ringing artifacts on the ^{103}Rh channel.

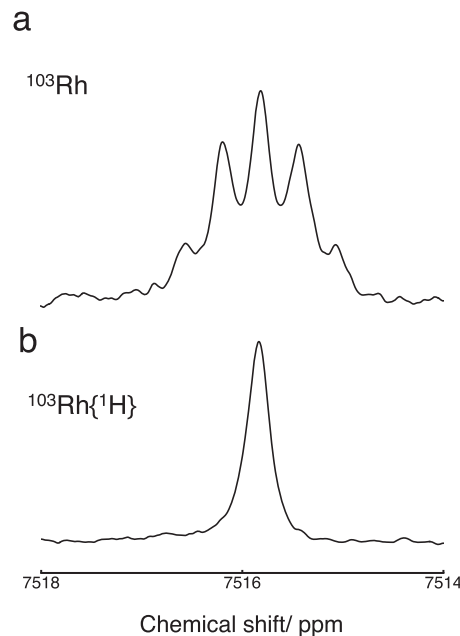


FIG. 7. (a) ^{103}Rh spectrum of a ~ 10 mM solution of rhodium formate in THF-d_8 scaled 2.5 times, acquired using 128 scans at 9.4 T and at 298 K using the pulse sequence in Fig. 6. (b) ^1H -decoupled ^{103}Rh spectrum acquired using 128 scans at 9.4 T and at 298 K using the pulse sequence in Fig. 6 with continuous-wave ^1H decoupling during signal acquisition. Acquisition time for each spectrum was 1 h. Exponential line broadening (1 Hz) was applied to each spectrum.

The rhodium formate ^{103}Rh spectrum features a single ^{103}Rh resonance split into a 1:4:6:4:1 pentet by couplings to the four equivalent ^1H nuclei on the formate ligands [Fig. 7(a)]. The three-bond ^1H - ^{103}Rh J-coupling is estimated to be $|^3J_{\text{RhH}}| = 4.7 \pm 0.1$ Hz, in agreement with the ^1H spectrum. The ^{103}Rh resonances collapse into a single peak centered at 7516 ppm upon ^1H decoupling [Fig. 7(b)].

The ^{103}Rh resonances are broadened by the short ^{103}Rh T_2 (see Fig. 13).

The ^{103}Rh chemical shift is temperature-dependent (see Fig. 8). The temperature-dependence of the ^{103}Rh chemical shift is approximately linear over the relevant temperature range, with a gradient of ~ 1.48 ppm K^{-1} . This is in general agreement with observations on similar Rh complexes.^{7,12}

3. Solid-state ^{13}C NMR

The chemical shift anisotropy (CSA) of the formate ^{13}C nuclei was estimated by magic-angle-spinning NMR experiments on rhodium formate solid (Fig. 9).

The estimated eigenvalues of the traceless, symmetric (rank-2) part of the shielding tensor are as follows: $\sigma_{xx}^{(2)} = 65.1$ ppm, $\sigma_{yy}^{(2)} = 5.5$ ppm, and $\sigma_{zz}^{(2)} = -70.7$ ppm. This corresponds to the following Frobenius norm of the rank-2 ^{13}C shielding tensor:

$$\begin{aligned} \|\sigma^{(2)}\|(^{13}\text{C}) &= \{(\sigma_{xx}^{(2)})^2 + (\sigma_{yy}^{(2)})^2 + (\sigma_{zz}^{(2)})^2\}^{1/2} \\ &= 96.3 \pm 1.0 \text{ ppm.} \end{aligned} \quad (5)$$

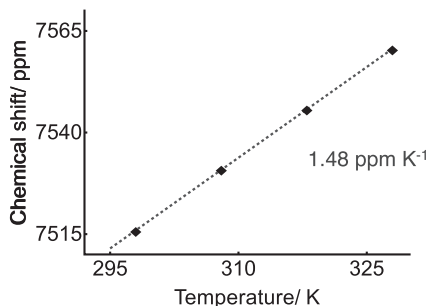


FIG. 8. ^{103}Rh chemical shift of rhodium formate dissolved in THF-d_8 at 9.4 T, as a function of temperature. The chemical shifts are referenced to $\Xi(^{103}\text{Rh}) = 3.16\%$.

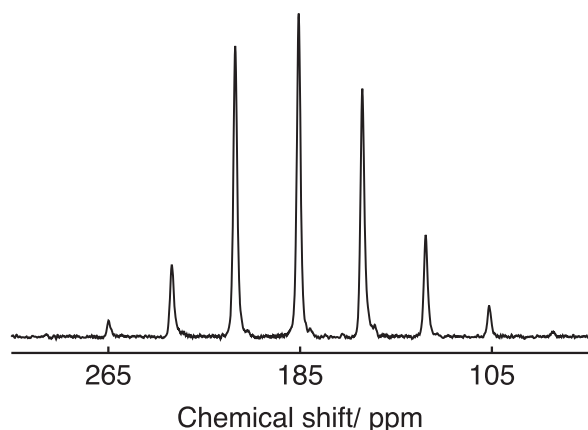


FIG. 9. Rhodium formate $^{13}\text{C}\{^1\text{H}\}$ solid-state CPMAS³⁶ NMR spectrum obtained at a spinning frequency of 4 kHz acquired using 2048 scans at 14.1 T and at 303 K. The chemical shift was referenced to adamantane. The contact time was 160 μs . The recycle delay was 3 s. ~ 150 mg of sample was used. Further details of the pulse sequence are provided in the supplementary material.

B. Relaxation times

1. ^1H -detected ^{103}Rh T_1

^{103}Rh T_1 relaxation time constants were measured indirectly through ^1H NMR signals using the sequence shown in Fig. 10. DualPol is used to transfer z-magnetization from the ^1H nuclei to the ^{103}Rh nuclei and allowed to relax toward equilibrium during the relaxation interval τ_{relax} . For field-dependent relaxation measurements, the sample is shuttled to a region of lower magnetic field during this interval, and back again. A proton destruction filter is applied to eliminate any residual proton magnetization, such as that generated during τ_{relax} through longitudinal relaxation toward equilibrium. Remaining ^{103}Rh z-magnetization, selected for by the two 90° pulses, is now transferred back to ^1H z-magnetization by a second DualPol block and is selected for by a proton z-filter. A final ^1H 90° pulse generates observable ^1H transverse magnetization. The sequence is repeated with variation of τ_{relax} in order to follow the equilibration of longitudinal ^{103}Rh magnetization.

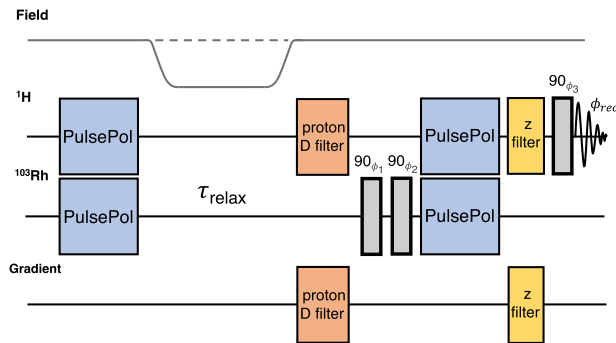


FIG. 10. Sequence used for the indirect measurement of rhodium T_1 through ^1H NMR signals. Phase cycles are given by $\phi_1 = [x, x, -x, -x]$, $\phi_2 = [-x, x, -x, x]$, $\phi_3 = [x, x, x, x, y, y, y, y, -x, -x, -x, -x, -y, -y, -y, -y]$ and the receiver $\phi_{\text{rec}} = [x, -x, -x, x, y, -y, -y, y, -x, x, x, -x, -y, y, y, -y]$. The optional shuttling of the sample to low field, and back again, during the interval τ_{relax} , is indicated.

The trajectory of indirectly detected ^{103}Rh z-magnetization in a field of 9.4 T is shown in Fig. 11(a). The trajectory fits well to a single-exponential decay with time constant $T_1(^{103}\text{Rh}) = 0.483 \pm 0.002$ s. A trajectory in the low magnetic field of 1 mT is shown in Fig. 11(b). This was produced by shuttling the sample to low magnetic field during the interval τ_{relax} . The relaxation process is much slower in low field, with a time constant of $T_1(^{103}\text{Rh}) = 28.2 \pm 1.2$ s.

The rhodium T_1^{-1} increases approximately quadratically with the magnetic field strength B , as shown in Fig. 11(c). The field-dependent relaxation rate constant is a reasonable fit to the quadratic function $T_1^{-1}(B) = T_1^{-1}(0) + aB^2$, where $T_1^{-1}(0) = 0.065 \pm 0.04$ s^{-1} and $a = 0.023 \pm 0.001$ $\text{s}^{-1} \text{T}^{-2}$.

2. ^1H -detected ^{103}Rh T_2

The sequence shown in Fig. 12 was used to measure the ^{103}Rh spin-spin relaxation time constant T_2 in high magnetic field.

Conversion of ^1H z-polarization into ^{103}Rh z-polarization is generated by a 90° pulse and allowed to decay during the subsequent spin echo of duration τ_{echo} . The ensuing 90° ^{103}Rh pulse returns the remaining transverse ^{103}Rh magnetization back to longitudinal ^{103}Rh polarization. A ^1H destruction filter destroys any residual ^1H magnetization before another DualPol cross-polarization block transfers ^{103}Rh z-magnetization back to ^1H z-magnetization. The ^1H z-filter selects for ^1H z-magnetization before the ^1H signal is induced by the final 90° ^1H pulse. The pulse sequence is repeated varying the echo delay τ_{echo} in order to follow the decay of ^{103}Rh transverse magnetization.

The trajectory of indirectly detected ^{103}Rh transverse magnetization in a field of 9.4 T is shown in Fig. 13. The trajectory fits well to a single-exponential decay with time constant $T_2(^{103}\text{Rh}) = 0.181 \pm 0.001$ s. Note that the measured value of T_2 is much smaller than T_1 under the same conditions.

3. ^{13}C inversion-recovery

As discussed below, the rotational correlation time τ_c of the rhodium formate complex may be estimated by a study of the ^{13}C longitudinal relaxation. These data were obtained by an indirect detection method exploiting the scalar-coupled formate protons, as

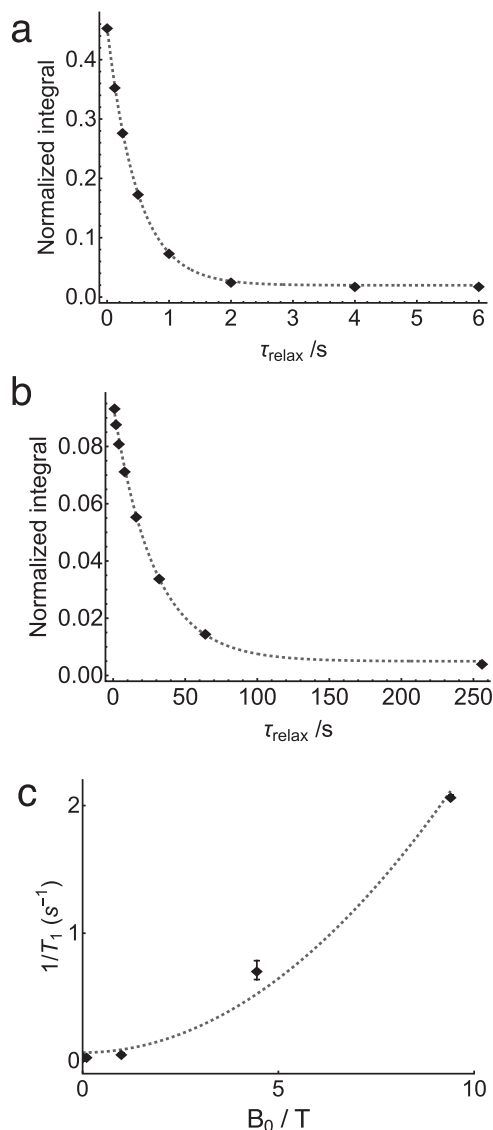


FIG. 11. (a) Decay curve for ^{103}Rh longitudinal magnetization at a field of 9.4 T, obtained using the pulse sequence in Fig. 10, but without shuttling the sample to low field. The data were acquired in ~ 20 min. The integrals are normalized against the ^1H spectrum obtained by a single ^1H 90° pulse applied to a system in thermal equilibrium at 9.4 T. The data fit well to an exponential decay with time constant $T_1 = 0.483 \pm 0.002$ s. (b) Decay curve for ^{103}Rh longitudinal magnetization at a field of 1 mT, obtained using the pulse sequence in Fig. 10, including the shuttling of the sample to low field. The data fit well to an exponential decay with time constant $T_1 = 28.2 \pm 1.2$ s. (c) ^{103}Rh relaxation rate constant T_1^{-1} as a function of magnetic field strength. The dashed line shows the quadratic function $T_1^{-1}(B) = T_1^{-1}(0) + aB^2$, where $T_1^{-1}(0) = 0.065 \pm 0.038 \text{ s}^{-1}$ and $a = 0.023 \pm 0.001 \text{ s}^{-1} \text{ T}^{-2}$.

described in the supplementary material. The inversion-recovery data fits well to a single-exponential recovery with a time constant of 2.64 ± 0.13 s for a solution in THF-d_8 , in a magnetic field of 9.4 T. However, as described below, the inversion-recovery curve for the

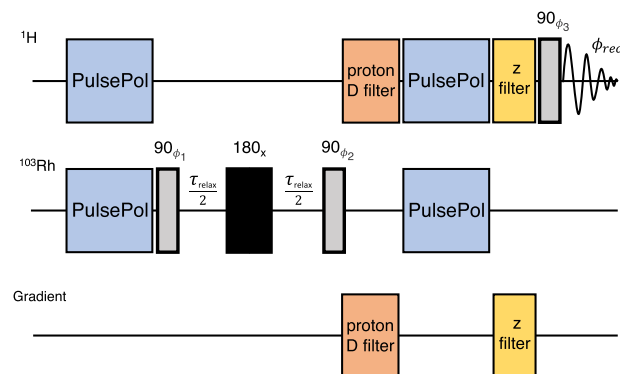


FIG. 12. Sequence used for the indirect measurement of rhodium T_2 with detection on protons. Phase cycles are given by $\phi_1 = [x, x, -x, -x]$, $\phi_2 = [-x, x, -x, x]$, $\phi_3 = [x, x, x, x, y, y, y, y, -x, -x, -x, -x, -y, -y, -y, -y]$ and the receiver $\phi_{\text{rec}} = [x, -x, -x, x, y, -y, -y, y, -x, x, x, -x, -y, y, y, -y]$. The black rectangle indicates a BB1 composite π -pulse [Eq. (3)].

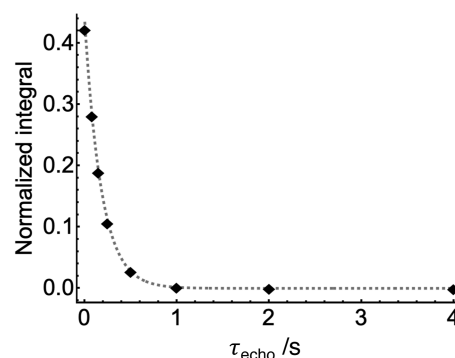


FIG. 13. Decay curve for ^{103}Rh transverse magnetization at a field of 9.4 T, obtained using the pulse sequence in Fig. 12. The data fit well to an exponential decay with time constant $T_2 = 0.181 \pm 0.001$ s. The integrals are normalized against the ^1H spectrum obtained by a single ^1H 90° pulse applied to a system in thermal equilibrium at 9.4 T.

^{13}C magnetization is best analyzed using a bi-exponential relaxation model.

IV. DISCUSSION

As shown in Fig. 11(c), the ^{103}Rh relaxation rate constant T_1^{-1} has a quadratic dependence on magnetic field B , with an additional zero-field contribution of $T_1^{-1}(0) = 0.0653 \pm 0.0383 \text{ s}^{-1}$. The quadratic field dependence is consistent with a dominant chemical shift anisotropy (CSA) relaxation mechanism, as is commonly observed for the ^{103}Rh NMR of rhodium complexes.^{12,37}

It is difficult to estimate the ^{103}Rh chemical shift anisotropy by solid-state NMR. The small magnetogyric ratio of ^{103}Rh and the very large CSA value make solid-state ^{103}Rh NMR very difficult. Our attempts to use the PROSPR method³⁸ to observe the ^{103}Rh spectrum indirectly in the solid state, by saturation transfer to the ^1H nuclei, were also unsuccessful. This is likely due to the very small dipole-dipole couplings between ^1H and ^{103}Rh nuclei in this

complex, which greatly inhibits dipolar-mediated polarization transfer in the solid state.

The symmetry of the complex indicates that the ^{103}Rh CSA tensors should have uniaxial symmetry ($\eta = 0$) with their unique principal axis along the Rh–Rh bond. This property is assumed in the following discussion.

Although the ^{103}Rh CSA may not be measured directly, it is possible to estimate it by a combination of field-dependent ^{103}Rh and ^{13}C T_1 measurements. The compact cage structure of the rhodium formate complex (Fig. 1) suggests that, to a good approximation, the complex tumbles in solution as a near-rigid body, with a common rotational correlation time τ_c for all spin interactions. This approximation allows a correlation time estimate from ^{13}C NMR to be applied in the context of ^{103}Rh NMR.

A ^{13}C nucleus of rhodium formate experiences two strong anisotropic interactions: the ^{13}C – ^1H dipole–dipole coupling with the directly bonded hydrogen nucleus and the ^{13}C chemical shift anisotropy. For point nuclei (i.e., ignoring the spatial spread of the nuclear wavefunctions), the ^{13}C – ^1H dipole–dipole coupling constant is given by $b_{CH} = -(\mu_0/4\pi)\hbar\gamma_C\gamma_H r_{CH}^{-3}$, where r_{CH} is the ^{13}C – ^1H internuclear distance.³⁹ Quantum chemical calculations³³ (see the supplementary material) predict an internuclear ^{13}C – ^1H distance of 1.097 Å, corresponding to a dipole–dipole coupling constant of $b_{CH} = -2\pi \times 22.8$ kHz. However, solid-state NMR studies have shown that the true dipole–dipole coupling is weakened by the angular spread of the ^1H wavefunctions, associated with the zero-point librational motion of the C–H bonds.⁴⁰ In the calculations below, we, therefore, assume a ^{13}C – ^1H dipole–dipole coupling constant of $b_{CH} = -2\pi \times (20.4 \pm 0.5)$ kHz.

For isolated ^{13}C – ^1H spin systems in the extreme narrowing approximation (fast tumbling), the theoretical recovery of ^{13}C longitudinal magnetization $M_z(t)$ after perturbation from equilibrium at time $t = 0$ is expected to follow the biexponential curve:

$$M_z(t) = M_z^{\text{eq}} + (M_z(0) - M_z^{\text{eq}}) \frac{1}{2} \left\{ \exp \left\{ - \left(\frac{1}{2} b_{CH}^2 + \frac{1}{5} \omega_{\text{CSA}}^2 \right) \tau_c \right\} + \exp \left\{ - \left(\frac{3}{2} b_{CH}^2 + \frac{1}{5} \omega_{\text{CSA}}^2 \right) \tau_c \right\} \right\}, \quad (6)$$

where M_z^{eq} is the thermal equilibrium ^{13}C magnetization, and ω_{CSA} is defined as follows:

$$\omega_{\text{CSA}} = -\gamma_C B_0 \|\boldsymbol{\sigma}^{(2)}\|, \quad (7)$$

where $\|\boldsymbol{\sigma}^{(2)}\|$ is the norm of the ^{13}C shielding tensor, as defined in Eq. (5). The biexponential form of Eq. (6) is due to ^1H – ^{13}C cross-relaxation during the magnetization recovery.^{41–43}

In a magnetic field of 9.4 T, the ^{13}C CSA, as estimated by ^{13}C solid-state NMR (Sec. III A 3), corresponds to an interaction strength of $\omega_{\text{CSA}} \approx 2\pi \times (9.7 \pm 0.1)$ kHz. By fitting the experimental ^{13}C inversion-recovery trajectory to an equation of the form in Eq. (6), we obtain the following estimate of the rotational correlation time for the rhodium formate paddlewheel complex in THF- d_8 solution at 298 K: $\tau_c \approx 24.5 \pm 1.5$ ps. The ^{103}Rh relaxation may now be analyzed using the estimate of τ_c from the ^{13}C data. As shown in Fig. 11, the ^{103}Rh T_1^{-1} relaxation rate constant is well-described by the function $T_1^{-1}(B) = T_1^{-1}(0) + aB^2$, with the field-independent term $T_1^{-1}(0) = 0.065 \pm 0.038 \text{ s}^{-1}$ and the quadratic coefficient $a = 0.023 \pm 0.001 \text{ s}^{-1} \text{ T}^{-2}$.

The quadratic field-dependent term may be ascribed to the CSA mechanism. In the extreme narrowing approximation (fast tumbling), the CSA contribution to the T_1^{-1} relaxation rate constant for ^{103}Rh is given by⁴³

$$(T_1^{-1}({}^{103}\text{Rh}))_{\text{CSA}}^{-1} = \frac{2}{15} B_0^2 \gamma_{\text{Rh}}^2 \Delta\sigma^2 \tau_c, \quad (8)$$

where the shielding anisotropy $\Delta\sigma$ is defined as follows:⁴³

$$\Delta\sigma = \frac{3}{2} (\sigma_{\text{ZZ}} - \sigma_{\text{iso}}) = -\frac{3}{2} \delta^{\text{aniso}}. \quad (9)$$

Equation (8) implies that the quadratic field-dependent coefficient a for the ^{103}Rh T_1^{-1} relaxation rate constant is given by

$$a = \frac{2}{15} \gamma_{\text{Rh}}^2 \Delta\sigma^2 \tau_c. \quad (10)$$

The experimental estimate of the quadratic coefficient $a = 0.023 \pm 0.001 \text{ s}^{-1} \text{ T}^{-2}$ may be combined with the correlation time estimate $\tau_c \approx 24.5 \pm 1.5$ ps to obtain the following experimental estimate of the ^{103}Rh shielding anisotropy: $|\Delta\sigma| = 9900 \pm 540$ ppm.

This is a very large number. Although prior estimates of the ^{103}Rh CSA are scarce in the literature, CSA values for heavy spin-1/2 nuclei are sometimes of a similar magnitude,^{44–53} with closely related platinum (II) compounds displaying ^{195}Pt CSA values on the order of 10 000 ppm.^{44,46,51,53} To our knowledge, the only other measurements of ^{103}Rh CSAs, in very different Rh(III) compounds, were on the order of ~ 500 – 1500 ppm.^{54,55} This dramatic range is also typical^{47,48,52} for heavy spin-1/2 nuclei.

Using ORCA,^{33,56,57} ^{103}Rh shielding tensors were computed at the TPSSh/SARC-ZORA-TZVPP level of theory using implicit solvation (CPCM^{58,59} for THF), the zeroth-order regular approximation (ZORA)^{60,61} for the inclusion of relativistic effects, Gauge-Independent Atomic Orbitals (GIAOs), the Resolution of Identity (RI) approximation,⁵⁷ and the tau-dependent correction as suggested by Dobson^{62–64} (see the supplementary material). The result is summarized in Table I.

The calculated CSA is somewhat smaller than the experimental estimate. Underestimation of CSAs calculated using the ZORA method has been reported for other heavy spin-1/2 nuclei,^{65–67} where better agreement might be obtained with higher order four-component relativistic calculations⁶⁶ or by accounting for the relativistic breakdown of the relationship between spin-rotation and the paramagnetic contribution to the anisotropy.⁶⁷

The origin of the zero-field contribution $T_1^{-1}(0)$ to the ^{103}Rh relaxation rate constant is currently unknown. As discussed in the supplementary material, the ^{103}Rh – ^{103}Rh and ^{103}Rh – ^1H

TABLE I. Estimates of the ^{103}Rh shielding tensor anisotropy $\Delta\sigma$ of Rh formate, defined in Eq. (9). The computational estimate is given by quantum chemical calculation using ORCA.³³ The experimental estimate is from the analysis of field-dependent ^{103}Rh relaxation in solution, as described in this paper.

Method	$ \Delta\sigma $ (ppm)
Calculated	7070
Experimental estimate	9900 ± 540

dipole–dipole couplings are much too weak to account for this term. In the literature, the low-field relaxation of heavy spin-1/2 nuclei is often^{6,68–70} attributed to a spin-rotation⁷¹ mechanism. However, to our knowledge, this conclusion has not been supported by any theoretical or computational studies.

The experimental estimate of the ^{103}Rh T_2 is much shorter than the estimate of T_1 under the same conditions ($T_2 = 0.181 \pm 0.001$ s as against $T_1 = 0.483 \pm 0.002$ s, in a field of 9.4 T. We tentatively attribute the short T_2 value to the modulation of the isotropic chemical shift by ligand exchange at the axial positions. Other decoherence mechanisms, such as diffusion in the presence of inhomogeneous magnetic fields, are expected to be too weak to account for the observed T_2 value in this case.

In conclusion, this paper has demonstrated methodology for the indirect estimation of ^{103}Rh T_1 and T_2 values by magnetization transfer to and from ^1H nuclei using the DualPol pulse sequence. Field-dependent ^{103}Rh T_1 measurements indicate a very large chemical shift anisotropy for the ^{103}Rh sites in the rhodium formate paddlewheel complex. The field-independent contribution to the ^{103}Rh relaxation rate constant is not fully understood at the current time.

A limitation of the methodology described here is the prerequisite of a spin system with direct scalar couplings between ^{103}Rh nuclei and a proton, which is not present in all rhodium complexes. This limitation may be addressed via the use of a relay nucleus, such as ^{13}C at natural abundance.^{7,72–74}

SUPPLEMENTARY MATERIAL

The supplementary material includes the ^{13}C relaxation data, experimental parameters for the solid-state ^{13}C spectrum, and details of the DFT calculations in ORCA.

ACKNOWLEDGMENTS

We acknowledge funding from the European Research Council (Grant No. 786707-FunMagResBeacons) and EPSRC-UK (Grant Nos. EP/P009980/1, EP/P030491/1, and EP/V055593/1). M.L. acknowledges financial support by the Max-Planck-Gesellschaft and the Max-Planck-Institut für Kohlenforschung. We thank Alexander A. Auer for advice on quantum chemical calculations. We thank Professor Brian E. Mann for advice and historical insights on rhodium NMR. We thank Alexey Kiryutin for sharing his designs for the sample shuttle.

AUTHOR DECLARATIONS

Conflict of Interest

The authors have no conflicts to disclose.

Author Contributions

Harry Harbor-Collins: Conceptualization (equal); Data curation (equal); Formal analysis (equal); Investigation (equal); Methodology (equal); Software (equal); Validation (equal); Visualization

(equal); Writing – original draft (equal); Writing – review & editing (equal). **Mohamed Sabba:** Conceptualization (equal); Data curation (equal); Formal analysis (equal); Investigation (equal); Methodology (equal); Software (equal); Visualization (equal); Writing – original draft (equal); Writing – review & editing (equal). **Gamal Moustafa:** Data curation (equal); Investigation (equal); Methodology (lead); Resources (lead); Validation (equal); Visualization (equal). **Bonifac Legrady:** Data curation (equal); Formal analysis (equal); Investigation (equal); Methodology (equal). **Murari Soundararajan:** Data curation (equal); Formal analysis (equal); Investigation (lead); Methodology (lead); Resources (lead). **Markus Leutzsch:** Conceptualization (lead); Investigation (lead); Validation (lead); Writing – review & editing (lead). **Malcolm H. Levitt:** Conceptualization (equal); Formal analysis (equal); Funding acquisition (equal); Investigation (equal); Project administration (equal); Resources (equal); Supervision (equal); Writing – original draft (equal); Writing – review & editing (equal).

DATA AVAILABILITY

The data that support the findings of this study are available from the corresponding author upon reasonable request.

REFERENCES

- 1 A. Erck, L. Rainen, J. Whaleyman, I.-M. Chang, A. P. Kimball, and J. Bear, “Studies of rhodium(II) carboxylates as potential antitumor agents,” *Proc. Soc. Exp. Biol. Med.* **145**, 1278–1283 (1974).
- 2 M. Fandzloch, A. W. Augustyniak, L. Dobrzańska, T. Jędrzejewski, J. Sitkowski, M. Wypij, and P. Golińska, “First dinuclear rhodium(II) complexes with triazolopyrimidines and the prospect of their potential biological use,” *J. Inorg. Biochem.* **210**, 111072 (2020).
- 3 J. Ohata and Z. T. Ball, “Rhodium at the chemistry–biology interface,” *Dalton Trans.* **47**, 14855–14860 (2018).
- 4 S. Lin and C. Turro, “Dirhodium complexes as panchromatic sensitizers, electrocatalysts, and photocatalysts,” *Chem. Eur. J.* **27**, 5379–5387 (2021).
- 5 R. Hrdina, “Dirhodium(II,II) paddlewheel complexes,” *Eur. J. Inorg. Chem.* **2021**, 501–528.
- 6 B. E. Mann, “The Cinderella nuclei,” *Annu. Rep. NMR Spectrosc.* **23**, 141–207 (1991).
- 7 F. P. Caló, G. Bistoni, A. A. Auer, M. Leutzsch, and A. Fürstner, “Triple resonance experiments for the rapid detection of ^{103}Rh NMR shifts: A combined experimental and theoretical study into dirhodium and bismuth–rhodium paddlewheel complexes,” *J. Am. Chem. Soc.* **143**, 12473–12479 (2021).
- 8 I. Schwartz, J. Scheuer, B. Tratzmiller, S. Müller, Q. Chen, I. Dhand, Z.-Y. Wang, C. Müller, B. Naydenov, F. Jelezko, and M. B. Plenio, “Robust optical polarization of nuclear spin baths using Hamiltonian engineering of nitrogen-vacancy center quantum dynamics,” *Sci. Adv.* **4**, eaat8978 (2018).
- 9 B. Tratzmiller, “Pulsed control methods with applications to nuclear hyperpolarization and nanoscale NMR,” Ph.D. thesis, Universität Ulm, 2021.
- 10 M. Sabba, N. Wili, C. Bengs, J. W. Whipham, L. J. Brown, and M. H. Levitt, “Symmetry-based singlet–triplet excitation in solution nuclear magnetic resonance,” *J. Chem. Phys.* **157**, 134302 (2022).
- 11 G. A. Rempel, P. Legzdins, H. Smith, G. Wilkinson, and D. A. Ucko, “Tetrakis(acetato)dirhodium(II) and similar carboxylato compounds,” in *Inorganic Syntheses* (John Wiley & Sons, Ltd., 1972), pp. 90–91.
- 12 L. Carlton, “Chapter 3–Rhodium-103 NMR,” *Annu. Rep. NMR Spectrosc.* **63**, 49–178 (2008).
- 13 G. C. Chingas, “Overcoupling NMR probes to improve transient response,” *J. Magn. Reson.* **54**, 153–157 (1983).
- 14 M. L. Buess and G. L. Petersen, “Acoustic ringing effects in pulsed nuclear magnetic resonance probes,” *Rev. Sci. Instrum.* **49**, 1151–1155 (1978).

- ¹⁵I. P. Gerathanassis, "Methods of avoiding the effects of acoustic ringing in pulsed Fourier transform nuclear magnetic resonance spectroscopy," *Prog. Nucl. Magn. Reson. Spectrosc.* **19**, 267–329 (1987).
- ¹⁶E. Fukushima and S. B. W. Roeder, "Spurious ringing in pulse NMR," *J. Magn. Reson.* **33**, 199–203 (1979).
- ¹⁷A. G. Redfield, "Shuttling device for high-resolution measurements of relaxation and related phenomena in solution at low field, using a shared commercial 500 MHz NMR instrument," *Magn. Reson. Chem.* **41**, 753–768 (2003).
- ¹⁸A. S. Kiryutin, A. N. Pravdivtsev, K. L. Ivanov, Y. A. Grishin, H.-M. Vieth, and A. V. Yurkovskaya, "A fast field-cycling device for high-resolution NMR: Design and application to spin relaxation and hyperpolarization experiments," *J. Magn. Reson.* **263**, 79–91 (2016).
- ¹⁹S. Wimperis, "Broadband, narrowband, and passband composite pulses for use in advanced NMR experiments," *J. Magn. Reson., Ser. A* **109**, 221–231 (1994).
- ²⁰H. K. Cummins, G. Llewellyn, and J. A. Jones, "Tackling systematic errors in quantum logic gates with composite rotations," *Phys. Rev. A* **67**, 042308 (2003).
- ²¹M. H. Levitt and R. Freeman, "NMR population inversion using a composite pulse," *J. Magn. Reson.* **33**, 473–476 (1979).
- ²²U. Haeberlen and J. S. Waugh, "Coherent averaging effects in magnetic resonance," *Phys. Rev.* **175**, 453–467 (1968).
- ²³E. R. P. Zuiderweg, "Analysis of multiple-pulse-based heteronuclear J cross polarization in liquids," *J. Magn. Reson.* **89**, 533–542 (1990).
- ²⁴B. Baishya and C. L. Khetrapal, "Perfect echo' INEPT: More efficient heteronuclear polarization transfer by refocusing homonuclear J -coupling interaction," *J. Magn. Reson.* **242**, 143–154 (2014).
- ²⁵R. T. Williamson, B. L. Márquez, W. H. Gerwick, and K. E. Kövér, "One- and two-dimensional gradient-selected HSQMBBC NMR experiments for the efficient analysis of long-range heteronuclear coupling constants," *Magn. Reson. Chem.* **38**, 265–273 (2000).
- ²⁶H. Koskela, I. Kilpeläinen, and S. Heikkinen, "Some aspects of quantitative 2D NMR," *J. Magn. Reson.* **174**, 237–244 (2005).
- ²⁷S. Gil, J. F. Espinosa, and T. Parella, "Accurate measurement of small heteronuclear coupling constants from pure-phase α/β HSQMBBC cross-peaks," *J. Magn. Reson.* **213**, 145–150 (2011).
- ²⁸H. Koskela, I. Kilpeläinen, and S. Heikkinen, "LR-CAHSQC: An application of a Carr–Purcell–Meiboom–Gill-type sequence to heteronuclear multiple bond correlation spectroscopy," *J. Magn. Reson.* **164**, 228–232 (2003).
- ²⁹M. H. Levitt and R. Freeman, "Composite pulse decoupling," *J. Magn. Reson.* **43**, 502–507 (1981).
- ³⁰M. Carravetta, M. Edén, X. Zhao, A. Brinkmann, and M. H. Levitt, "Symmetry principles for the design of radiofrequency pulse sequences in the nuclear magnetic resonance of rotating solids," *Chem. Phys. Lett.* **321**, 205–215 (2000).
- ³¹S. J. Glaser and J. J. Quant, "Homonuclear and heteronuclear Hartmann–Hahn transfer in isotropic liquids," *Adv. Magn. Opt. Reson.* **19**, 59–252, 253e–254e (1996).
- ³²G. Wider, V. Dotsch, and K. Wuthrich, "Self-compensating pulsed magnetic-field gradients for short recovery times," *J. Magn. Reson., Ser. A* **108**, 255–258 (1994).
- ³³F. Neese, F. Wennmohs, U. Becker, and C. Riplinger, "The ORCA quantum chemistry program package," *J. Chem. Phys.* **152**, 224108 (2020).
- ³⁴S. Zhang, X. Wu, and M. Mehring, "Elimination of ringing effects in multiple-pulse sequences," *Chem. Phys. Lett.* **173**, 481–484 (1990).
- ³⁵F. Wang, S. K. Ramakrishna, P. Sun, and R. Fu, "Triple-pulse excitation: An efficient way for suppressing background signals and eliminating radio-frequency acoustic ringing in direct polarization NMR experiments," *J. Magn. Reson.* **332**, 107067 (2021).
- ³⁶B. H. Meier, "Cross polarization under fast magic angle spinning: Thermodynamical considerations," *Chem. Phys. Lett.* **188**, 201–207 (1992).
- ³⁷M. Cocivera, G. Ferguson, R. E. Lenkinski, P. Szczecinski, F. J. Lalor, and D. J. O'Sullivan, "NMR relaxation studies of ^{103}Rh ," *J. Magn. Reson.* **46**, 168–171 (1982).
- ³⁸M. J. Jaroszewicz, A. R. Altenhof, R. W. Schurko, and L. Frydman, "Sensitivity enhancement by progressive saturation of the proton reservoir: A solid-state NMR analogue of chemical exchange saturation transfer," *J. Am. Chem. Soc.* **143**, 19778–19784 (2021).
- ³⁹M. H. Levitt, *Spin Dynamics. Basics of Nuclear Magnetic Resonance*, 2nd ed. (Wiley, Chichester, 2007).
- ⁴⁰T. Nakai, J. Ashida, and T. Terao, "Influence of small-amplitude motions on two-dimensional N.M.R. powder patterns," *Mol. Phys.* **67**, 839–847 (1989).
- ⁴¹I. Solomon, "Relaxation processes in a system of two spins," *Phys. Rev.* **99**, 559–565 (1955).
- ⁴²T. D. Alger, R. Freeman, and D. M. Grant, "Carbon-13 T_1 measurements under proton coupled and decoupled conditions," *J. Chem. Phys.* **57**, 2168–2171 (1972).
- ⁴³J. Kowalewski and L. Mäler, *Nuclear Spin Relaxation in Liquids Theory, Experiments, and Applications*, 2nd ed. (CRC Press, Taylor & Francis Group, Boca Raton, FL, 2018).
- ⁴⁴J. J. Dechter and J. Kowalewski, " ^{195}Pt spin-lattice relaxation and shielding anisotropy for $\text{Pt}(\text{acac})_2$," *J. Magn. Reson.* **59**, 146–149 (1984).
- ⁴⁵P. Paluch, A. G. M. Rankin, J. Trébosc, O. Lafon, and J.-P. Amoureux, "Analysis of HMQC experiments applied to a spin $\frac{1}{2}$ nucleus subject to very large CSA," *Solid State Nucl. Magn. Reson.* **100**, 11–25 (2019).
- ⁴⁶S. W. Sparks and P. D. Ellis, "Platinum-195 shielding tensors in potassium hexachloroplatinate(IV) and potassium tetrachloroplatinate(II)," *J. Am. Chem. Soc.* **108**, 3215–3218 (1986).
- ⁴⁷A. Venkatesh, A. Lund, L. Rochlitz, R. Jabbour, C. P. Gordon, G. Menzildjian, J. Viger-Gravel, P. Berruyer, D. Gajan, C. Copéret, A. Lesage, and A. J. Rossini, "The structure of molecular and surface platinum sites determined by DNP-SENS and fast MAS ^{195}Pt solid-state NMR spectroscopy," *J. Am. Chem. Soc.* **142**, 18936–18945 (2020).
- ⁴⁸R. Benn, H. Michael Büch, and R.-D. Reinhardt, "Heavy metal spin- $\frac{1}{2}$ nuclei. Platinum-195 relaxation times in phosphorus-platinum(o) compounds and their dependence on the geometry of the complex," *Magn. Reson. Chem.* **23**, 559–564 (1985).
- ⁴⁹A. Bagno and R. Bini, "NMR spectra of terminal oxo gold and platinum complexes: Relativistic DFT predictions," *Angew. Chem., Int. Ed.* **49**, 1083–1086 (2010).
- ⁵⁰F. A. Perras, A. Venkatesh, M. P. Hanrahan, T. W. Goh, W. Huang, A. J. Rossini, and M. Pruski, "Indirect detection of infinite-speed MAS solid-state NMR spectra," *J. Magn. Reson.* **276**, 95–102 (2017).
- ⁵¹A. Venkatesh, M. J. Ryan, A. Biswas, K. C. Boteju, A. D. Sadow, and A. J. Rossini, "Enhancing the sensitivity of solid-state NMR experiments with very low gyromagnetic ratio nuclei with fast magic angle spinning and proton detection," *J. Phys. Chem. A* **122**, 5635–5643 (2018).
- ⁵²A. Venkatesh, D. Giofrè, B. A. Atterberry, L. Rochlitz, S. L. Carnahan, Z. Wang, G. Menzildjian, A. Lesage, C. Copéret, and A. J. Rossini, "Molecular and electronic structure of isolated platinum sites enabled by the expedient measurement of ^{195}Pt chemical shift anisotropy," *J. Am. Chem. Soc.* **144**, 13511–13525 (2022).
- ⁵³A. Venkatesh, F. A. Perras, and A. J. Rossini, "Proton-detected solid-state NMR spectroscopy of spin-1/2 nuclei with a large chemical shift anisotropy," *J. Magn. Reson.* **327**, 106983 (2021).
- ⁵⁴H. Adams, N. A. Bailey, B. E. Mann, B. F. Taylor, C. White, and P. Yavari, "Activation energies for molecular tumbling and cyclopentadienyl rotation in $[\text{M}(\eta^5\text{-C}_5\text{H}_5)(\eta^4\text{-cod})]$ ($\text{M} = \text{Rh}$ or Ir ; $\text{cod} = \text{cyclo-octa-1,5-diene}$) and the X-ray crystal structure of and bonding in $[\text{Rh}(\eta^5\text{-C}_5\text{H}_5)(\eta^4\text{-cod})]$," *J. Chem. Soc., Dalton Trans.* **1987**, 1947–1951.
- ⁵⁵B. L. Phillips, J. R. Houston, J. Feng, and W. H. Casey, "Observation of solid-state ^{103}Rh NMR by cross-polarization," *J. Am. Chem. Soc.* **128**, 3912–3913 (2006).
- ⁵⁶G. L. Stoychev, A. A. Auer, R. Izsák, and F. Neese, "Self-consistent field calculation of nuclear magnetic resonance chemical shielding constants using gauge-including atomic orbitals and approximate two-electron integrals," *J. Chem. Theory Comput.* **14**, 619–637 (2018).
- ⁵⁷G. L. Stoychev, A. A. Auer, and F. Neese, "Efficient and accurate prediction of nuclear magnetic resonance shielding tensors with double-hybrid density functional theory," *J. Chem. Theory Comput.* **14**, 4756–4771 (2018).
- ⁵⁸V. Barone and M. Cossi, "Quantum calculation of molecular energies and energy gradients in solution by a conductor solvent model," *J. Phys. Chem. A* **102**, 1995–2001 (1998).
- ⁵⁹M. Garcia-Ratés and F. Neese, "Effect of the solute cavity on the solvation energy and its derivatives within the framework of the Gaussian charge scheme," *J. Comput. Chem.* **41**, 922–939 (2020).

- ⁶⁰R. Bouten, E. J. Baerends, E. van Lenthe, L. Visscher, G. Schreckenbach, and T. Ziegler, "Relativistic effects for NMR shielding constants in transition metal oxides using the zeroth-order regular approximation," *J. Phys. Chem. A* **104**, 5600–5611 (2000).
- ⁶¹C. van Wüllen, "Molecular density functional calculations in the regular relativistic approximation: Method, application to coinage metal diatomics, hydrides, fluorides and chlorides, and comparison with first-order relativistic calculations," *J. Chem. Phys.* **109**, 392–399 (1998).
- ⁶²J. F. Dobson, "Alternative expressions for the Fermi hole curvature," *J. Chem. Phys.* **98**, 8870–8872 (1993).
- ⁶³S. Reimann, U. Ekström, S. Stopkowitz, A. M. Teale, A. Borgoo, and T. Helgaker, "The importance of current contributions to shielding constants in density-functional theory," *Phys. Chem. Chem. Phys.* **17**, 18834–18842 (2015).
- ⁶⁴C. J. Schattenberg and M. Kaupp, "Effect of the current dependence of tau-dependent exchange-correlation functionals on nuclear shielding calculations," *J. Chem. Theory Comput.* **17**, 1469–1479 (2021).
- ⁶⁵F. Alkan and C. Dybowski, "Spin-orbit effects on the ¹²⁵Te magnetic-shielding tensor: A cluster-based ZORA/DFT investigation," *Solid State Nucl. Magn. Reson.* **95**, 6–11 (2018).
- ⁶⁶J. Autschbach, "The accuracy of hyperfine integrals in relativistic NMR computations based on the zeroth-order regular approximation," *Theor. Chem. Acc.* **112**, 52–57 (2004).
- ⁶⁷E. Malkin, S. Komarovskiy, M. Repisky, T. B. Demissie, and K. Ruud, "The absolute shielding constants of heavy nuclei: Resolving the enigma of the ¹¹⁹Sn absolute shielding," *J. Phys. Chem. Lett.* **4**, 459–463 (2013).
- ⁶⁸R. Benn, H. Brenneke, and R.-D. Reinhardt, "¹⁰³Rh-NMR bei 9,4 T-verbessertes Nachweis infolge verkürzter relaxationszeiten und selektivem polarisationstransfer/¹⁰³Rh NMR at 9.4 T-improved signal detection due to shortened relaxation times and selective polarisation transfer," *Z. Naturforsch., B* **40**, 1763–1765 (1985).
- ⁶⁹R. Benn and A. Ruffinska, "High-resolution metal NMR spectroscopy of organometallic compounds [new analytical methods (30)]," *Angew. Chem., Int. Ed.* **25**, 861–881 (1986).
- ⁷⁰A. Hafner, W. von Philipsborn, and A. Schwenk, "Mechanisms for the longitudinal and transverse relaxation of iron-57," *J. Magn. Reson.* **74**, 433–449 (1987).
- ⁷¹D. E. Korenchan, J. Lu, M. Sabba, L. Dagys, L. J. Brown, M. H. Levitt, and A. Jerschow, "³¹P spin-lattice and singlet order relaxation mechanisms in pyrophosphate studied by isotopic substitution, field shuttling NMR, and molecular dynamics simulation," *Phys. Chem. Chem. Phys.* **24**, 24238–24245 (2022).
- ⁷²R. Benn and A. Ruffinska, "Indirect two-dimensional heteronuclear NMR spectroscopy of low- γ metal nuclei ($M = ^{183}\text{W}, ^{57}\text{Fe}, ^{103}\text{Rh}, ^{61}\text{Ni}$)," *Magn. Reson. Chem.* **26**, 895–902 (1988).
- ⁷³H. C. E. McFarlane, W. McFarlane, and D. S. Rycroft, "Studies of tungsten-183 magnetic shielding by heteronuclear magnetic double and triple resonance," *J. Chem. Soc., Dalton Trans.* **1976**, 1616–1622.
- ⁷⁴S. Weske, Y. Li, S. Wiegmann, and M. John, "H(C)Ag: A triple resonance NMR experiment for ¹⁰⁹Ag detection in labile silver-carbene complexes: NMR experiment for ¹⁰⁹Ag detection in labile silver-carbene complexes," *Magn. Reson. Chem.* **53**, 291–294 (2015).